2009 American WJTA Conference and Expo
August 18-20, 2009 ● Houston, Texas

Paper

OBSERVATIONS OF TITANIUM SURFACES IMPINGED WITH ULTRA-HIGH PRESSURE WATERJETS

Alex Chillman* and M. Ramulu
Department of Mechanical Engineering, Box 352600
University of Washington, Seattle, WA 98105

M. Hashish
Flow International Corporation
Kent, WA 98032

ABSTRACT

Over the past decades, waterjet processing has become a viable alternative to conventional material removal methods such as chemical milling or grinding. In full, waterjets have exhibited capabilities for cutting, surface texturing, cleaning, material removal, and peening processes – many of which fall into the field of surface preparation. As material advancements continue, research into alternate surface processing methods must strive to keep pace. One material in particular that has experienced an increase in use in the biomedical and aerospace industries is titanium – due largely to its high strength to weight ratio and corrosion resistance. In this study, a waterjet was used to process a titanium alloy at pressures ranging from 275 MPa (40 ksi) to 600 MPa (87 ksi) to characterize the erosion rates based on (i) supply pressure, (ii) traverse rate, and (iii) standoff distance. The erosion rates, resulting surface roughness parameters, and erosion widths were analyzed using optical methods and white light scanning electroscopy. Based on the results of this study, a need exists for a means of minimizing the stochastic nature of the waterjet removal process with respect to erosion width and removal rates. One solution is reducing the traverse rate, but another that has shown promise is the use of the fuzzy waterjet, or water-air jet. Preliminary results for the fuzzy waterjet show that a strong potential exists for uniform material removal at increased processing speeds.

* Research Engineer at Flow International Corporation

1. INTRODUCTION

High-pressure waterjets (WJ) at pressures up to 400 MPa have been commercialized for water-only surface preparation processes including coating removal, surface texturing, and waterjet cleaning. Also waterjet peening is rapidly emerging. While waterjets are commonly used for paint stripping, a need exists for improved processing of hard-to-machine coating and substrate materials. Increased operating pressure is one strategy to further advance the effectiveness of the waterjet for surface treatment processes [1-2]. The following are the advantages that may be obtained when waterjet operation occurs at increased pressures:

- Increase surface processing speeds
- Reduce processing cost
- Reduce water consumption
- Increase power density of the jet
- Remove harder coatings
- Texture hard-to-machine materials
- Reduce exposure time for waterjet peening

The objective of this study was to quantify the erosion characteristics and resulting surfaces generated on a titanium alloy using high-pressure waterjets. The key process parameters of interest were supply pressure, traverse rate, and standoff distance – with an initial look into the addition of air into the jet stream using the fuzzy jet, or water-air jet (WAJ) [3]. The WAJ is formed by either injecting or entraining a secondary fluid into a mixing chamber to cause an accelerated breakdown of the jet stream. The water-air jet has been screened experimentally for both peening and material removal considerations [4-8].

2. EXPERIMENTAL CONDITIONS AND PROCEDURE

2.1 Materials and Preparation

Commercial titanium alloy Ti-6Al-4V sheet material was utilized in this experimental study. The specimens were machined from conventional grain sheet, with the final dimension of 254 mm x 38.1 mm x 3.2 mm thick. Each sample was polished using 180 grit, 240 grit, 320 grit, and 400 grit emery paper until no visible scratches exist in any orientation other than the direction of polish. The polished specimen average roughness (R_a) was 0.5 micron.

2.2 Experimental Procedure and Analysis

The high-pressure WJ system used for this investigation was driven by a FLOW HyperJet intensifier pump capable of generating supply pressures up to 600 MPa. This system is capable of producing a flow rate of 5.3 liters/min at 600 MPa. The pressurized water was transferred through a stainless steel plumbing run, and then directed through a diamond orifice. The round waterjet nozzle employed an orifice with a diameter of 0.254 mm, which exhibited a coefficient of discharge (C_D) of 0.69 based on flow rate testing. An image of the free standing jet operating at 600 MPa can be seen in Figure 1.

Figure 1. Image depicting jet structure for a WJ operating at 600 MPa. *(Scale in inches)*

Table 1 lists the range of variables considered for this study. A total of 83 independent experimental runs were performed, with 10 repetitive sets to fully characterize the generated surfaces. The details of the experimental processing are listed in Table 2 - Table 4. The testing was performed in three distinct sets. The initial set of experiments (Set #1) considered a low-mid-high factorial approach, however it was found the standoff range considered was inadequate. Set #2 provided an expanded look at the effects of standoff distance. Set #3 was performed to further characterize the parametric effects at the various pressure/traverse rate combinations.

Table 1. WJ surface preparation conditions.

Nozzle Type	Round Jet (WJ)
Pressure (P_S)	275 – 600 MPa
Traverse Rate (u)	30 – 150 mm/s
SOD Range (h)	12.7 – 139.7 mm

In all experiments, the nozzle was oriented perpendicular to the target material. The nozzle traversed perpendicular to the rolling direction of the titanium sheet. The standoff distances were obtained by raising the nozzle until the appropriate nozzle–to–surface distance was achieved.

All of the treated surfaces were examined by optical microscopy and non-contact laser scanning to characterize the volume removal. Optical examination took place on a Keyence VHX 600 system, using a 20 – 200x lens. The erosion volumes were characterized by analyzing the treated surface using a ZYGO NewView 7300 non-contact 3D measurement system which utilized scanning white light interferometry. The analysis was performed using a 5x objective in conjunction with a 0.5x discrete zoom. The erosion volumes were determined by utilizing a 'volume down' function, which allows the user to generate a reference plane (in this case the non-treated specimen surface), and calculate the volume of material removed below. The scan size for each measurement was 1.2 mm wide by 2.12 mm long. Three measurements were taken

for each individual process condition to highlight the scatter due to the stochastic nature of the WJ material removal process. The roughness parameters were also determined for the centerline of the erosion track. An analysis of variance (ANOVA) was performed on the erosion rate results, as well as the average and peak to valley roughness parameters. Relative contributions of the process parameters on the dependent variables were evaluated. Linear and quadratic effects were considered in the ANOVA. Non-linear regression models were developed for the dependent variables in terms of the treatment parameters using a commercial statistical package (FusionPro). Parameters with insignificant effect were identified from the ANOVA ($\leq 3\%$), and excluded from the model.

The variation in erosion width was also identified for the generated surfaces. An initial look into an alternate processing means, the fuzzy waterjet or water-air jet, was performed to determine how injecting air into the waterjet stream affected the variations in erosion width.

3. RESULTS

Figure 2 shows the optical micrographs of the Ti–6Al–4V surfaces exposed to the WJ, with the arrows highlighting the direction of nozzle traverse. For h = 25.4 mm, limited erosion was evident. Only small isolated pockets of erosion exist. As the standoff distance increased to 76.2 mm, erosion became evident. Note that the erosion width varied considerably, as shown in the second column of Figure 2, and the erosion was clearly stochastic in nature. As the standoff distance was further increased to 127 mm, the coverage of the erosion zones began to dissipate further.

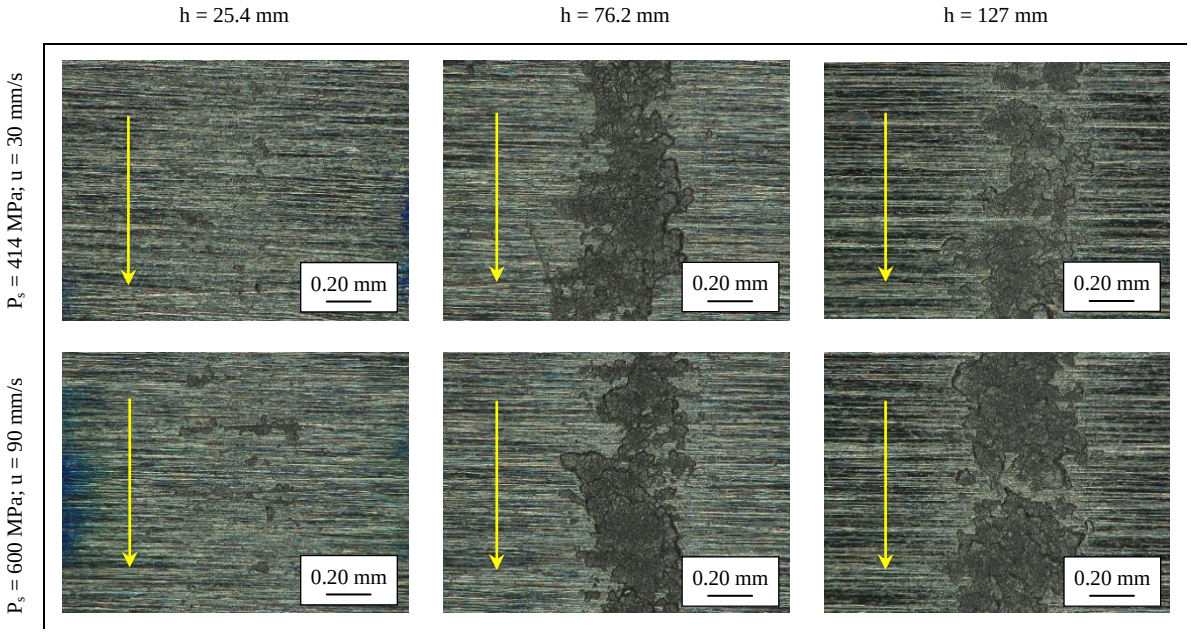

Figure 2. Optical micrographs of WJ processed surfaces.

Figure 3 (a) and (b) highlight the scanned 3D surface image from the Zygo analysis on the Ti–6Al–4V specimen prepared with P_S = 600 MPa, h = 38.1 mm, and u = 90 mm/s. The arrows indicate the direction of nozzle traverse. Small isolated pockets of erosion existed, which agrees

with the micrographs shown in Figure 2. Further analysis shows that the maximum depth of the pits was 20 µm, with a total volume of 0.0013 mm^3 removed over the 2.12 mm scan length. Figure 3 (c) and (d) show that as the traverse rate decreased to 30 mm/s, the erosion became much more uniform from a coverage standpoint, with the depth reaching 50 µm. The total volume removed also increased to 0.0189 mm^3.

Analysis of three locations on each of the 83 test cases was performed, and the total volume removed over a 2.12 mm scan length was determined for each processed region. The average values for the erosion volume, peak to valley roughness, average roughness, and erosion width were determined. From this data, material erosion rates were calculated by using E.R. = $(Vol_{Removed}*u)/L_{scan}$.

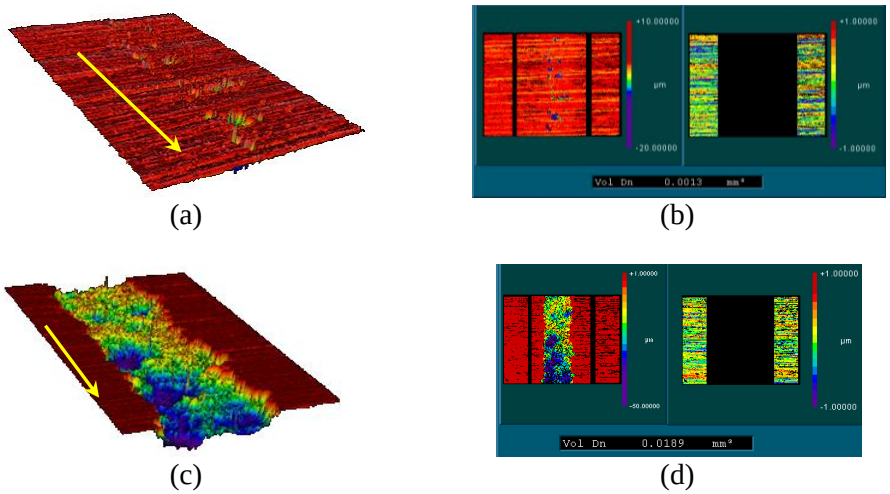

(a) (b)

(c) (d)

Figure 3. 3D images and volume removal analysis for the cases of P_s = 600 MPa and h = 38.1 mm, with a traverse rate of (a)/(b) u = 90 mm/s and (c)/(d) u = 30 mm/s.

An analysis of variance (ANOVA) was performed on the erosion rate measurements to identify the dominant process parameters. Results from the ANOVA for the erosion rates are shown in Figure 4 (a), and based on the relative contributions the influential factors were identified. It should be noted that the supply pressure and the traverse rate were the most influential parameters. An empirical model was determined for the erosion rate, and is given by:

$$E.R. = e^{(E.R.)'} \tag{1}$$

with (E.R.)' defined by:

$$\begin{aligned}(E.R.)' = {} & -6.92 - (1.06 * 10^{-3})P_S + (4 * 10^{-2})\,h + (1.52 * 10^{-2})\,u + (1.4 * 10^{-5})\,P_S{}^2 \\ & - (2.9 * 10^{-4})\,h^2 + (7.2 * 10^{-5})\,u^2 + (4.8 * 10^{-5})(P_S * h) - (8 * 10^{-5})(P_S * u) \\ & - (1.4 * 10^{-4})(h * u)\end{aligned} \tag{2}$$

where P_S, h, and u relate to the supply pressure, standoff distance, and traverse rate, respectively. A high degree of correlation (R^2 = 0.92) was obtained between the model and the 83 experimental measurements, with an error of 2.2%. Using Equations (1) and (2), the influence of the supply pressure and standoff distance were highlighted for the case of a u = 30 mm/s in Figure 4 (b). Figure 4 (b) indicates that the erosion rate increased with increasing supply

pressure. At small standoff distances, minimal erosion is expected, which agrees with the results of the optical analysis.

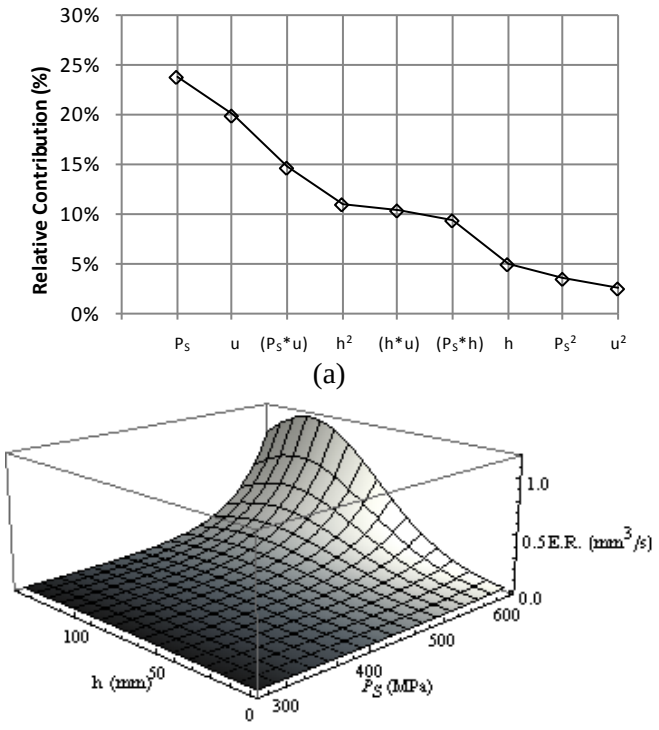

Figure 4. Erosion Rate: (a) Relative contributions and (b) Response surface highlighting influence of P_S and h. The response surface was developed for u = 30 mm/s.

A further analysis of the influence of traverse rate can be performed by considering the contour plots generated at various traverse rates, shown Figure 5. Two key trends can be highlighted from these figures: (i) as the pressure increased, the erosion rate increased for all traverse rates, (ii) as the traverse rate increased, the maximum attainable erosion rate decreased.

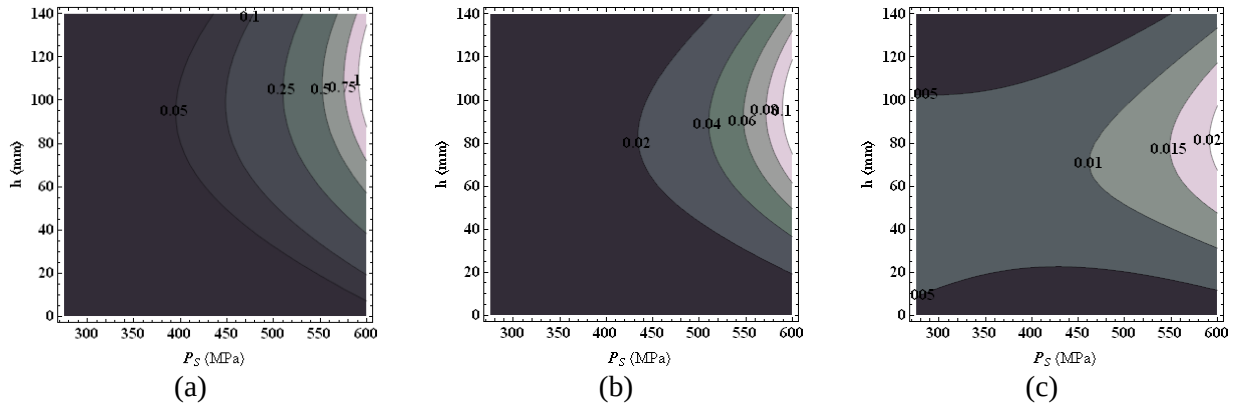

Figure 5. Contour plots highlighting erosion rate for (a) 30 mm/s, (b) 90 mm/s, and (c) 150 mm/s traverse rates.

The ANOVA results can be further explored to determine the relative effect the process parameters had on the resulting surface roughness parameters. Both the average surface

roughness (R_a) and peak-to-valley roughness (R_y) were considered in this study. The relative contributions of the process parameters on R_a are shown in Figure 6 (a). Pressure and traverse rate displayed the most substantial impact on R_a. A non-linear regression model was developed to define R_a, which is given by:

$$R_a = e^{(R_a)'} \tag{3}$$

where:

$$(R_a)' = -4.78 + (8.09 * 10^{-3})P_S + (3.66 * 10^{-2})\,h + (2.13 * 10^{-2})\,u - (2.27 * 10^{-4})\,h^2 + (4.4 * 10^{-5})(P_S * h) - (6.1 * 10^{-5})(P_S * u) - (1.62 * 10^{-4})(h * u) \tag{4}$$

A correlation coefficient of 0.85 was obtained, with an error of 3.9%. Using Equations (3) and (4), the influence of supply pressure and standoff distance on R_a can be represented by the response surface, shown in Figure 6 (b). Note that the average roughness increased with increasing supply pressure.

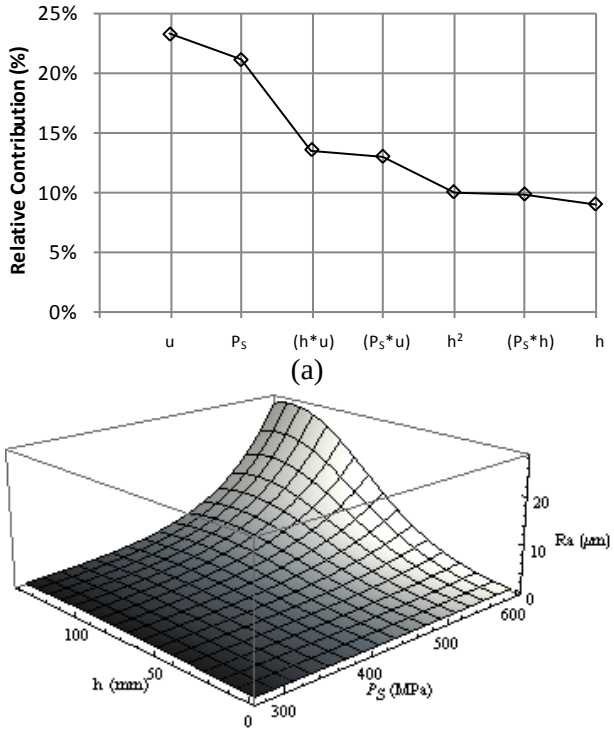

Figure 6. R_a: (a) Relative contributions and (b) Response surface highlighting influence of P_S and h. The response surface was developed for u = 30 mm/s.

Similarly, the peak to valley roughness can be evaluated based on the ANOVA results. The relative contributions of the process parameters can be found in Figure 7 (a). Again, the supply pressure and traverse rate were they most influential parameters. R_y can be defined by the exponential empirical model:

$$R_y = e^{(R_y)'} \tag{5}$$

where:

$$\left(R_y\right)' = -0.687 + (1 * 10^{-4})\mathrm{P_S} + (4.4 * 10^{-2})\,\mathrm{h} + (1.1 * 10^{-2})\,\mathrm{u} + (9 * 10^{-6})\,{\mathrm{P_S}}^2 - (1.92 * 10^{-4})(\mathrm{h}^2) - (4 * 10^{-5})(\mathrm{P_S} * \mathrm{u}) - (9.9 * 10^{-5})(\mathrm{h} * \mathrm{u}) \quad (6)$$

The comparison of the quadratic regression analysis to the experimental results yields a correlation factor of 0.85, with an error of 8%. The resulting expression can be evaluated to generate the response surface highlighting the influence of supply pressure and standoff distance on R_y, as shown in Figure 7 (b). R_y increased with increasing pressure. The trend with respect to standoff distance showed an increase in R_y up to a maximum value of 80 µm at h = 90 mm; with the roughness decreasing as the standoff distance continued to increase further.

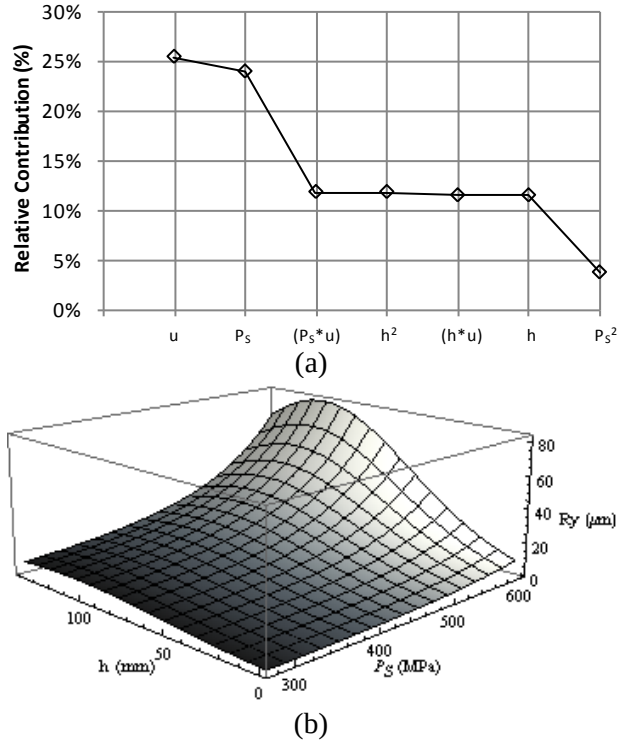

Figure 7. R_y: (a) Relative contributions and (b) Response surface highlighting influence of P_S and h. The response surface was developed for u = 30 mm/s.

Another key parameter of the waterjet erosion process is the erosion width. Figure 8 depicts the erosion width versus standoff distance relationship using P_S = 600 MPa and u = 90 mm/s. Graphically, the data points represent the average of nine measurements spaced over the length of the erosion track. The erosion width varied greatly for the case of water-only material removal at a 90 mm/s traverse rate, as seen in Figure 8 (a).

A preliminary study was performed to characterize the effect of injecting air into the cutting stream to form a water-air jet, or fuzzy waterjet. For the fuzzy waterjet experiments, a mixing tube 25.4 mm long and 0.762 mm diameter was used downstream of the orifice. The air was injected into a small mixing chamber located immediately below of the orifice. When an air flow (q_a) of 0.06 m^3/min was injected into the jet stream, the erosion width became far more

uniform for u = 90 mm/s, as depicted in Figure 8 (b). The erosion width also increased to the 0.5 – 0.6 mm range. As the air flow rate continued to increase (Figure 8 (c)), the variations in erosion width again increased for standoff distances greater than 38.1 mm.

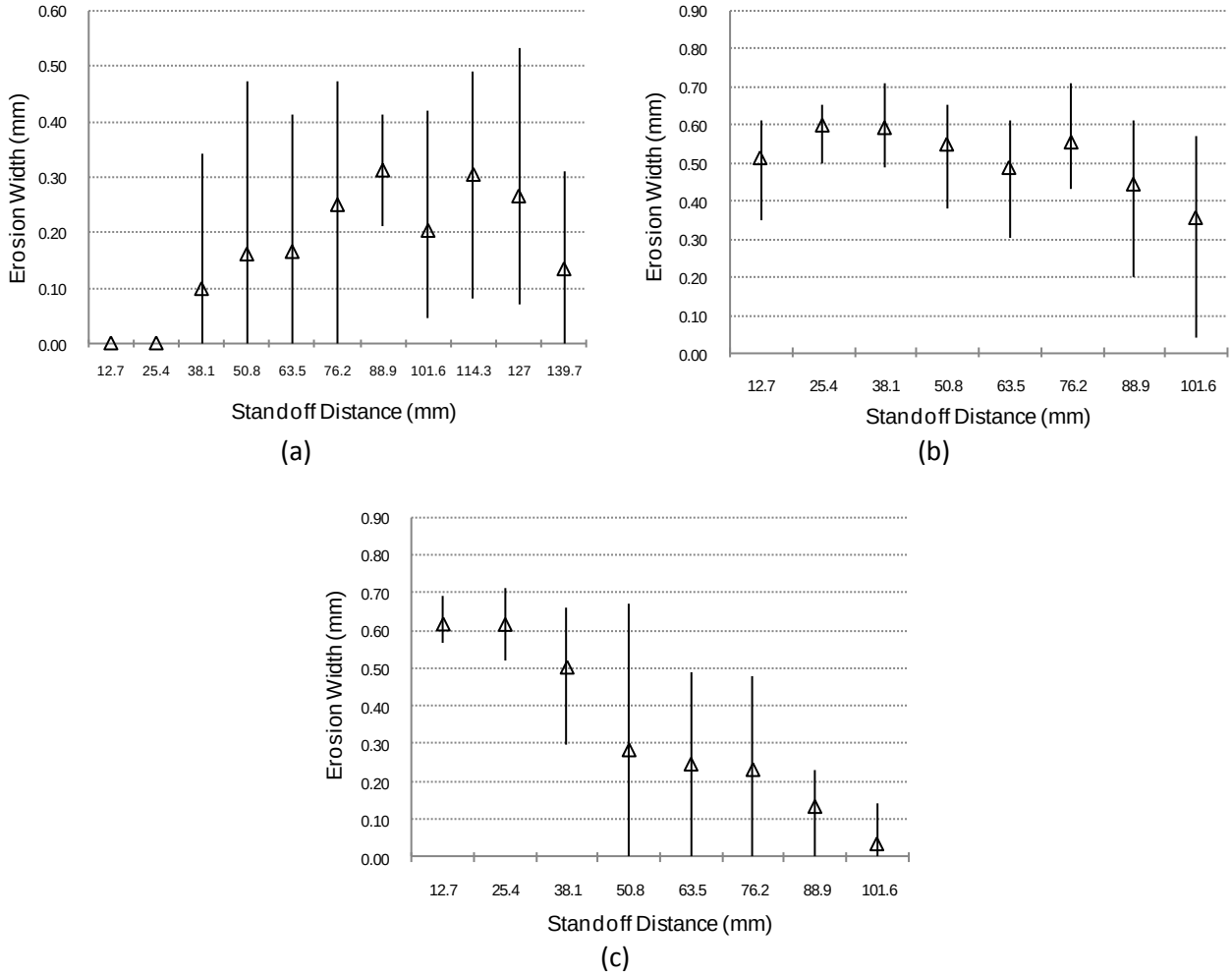

Figure 8. Erosion width – standoff distance relationship for specimens prepared using P_S = 600 MPa, u = 90 mm/s, and (a) WJ nozzle (b) WAJ with q_a = 0.06 m^3/min (c) WAJ with q_a = 0.16 m^3/min.

4. CONCLUSIONS

A study of the parametric effects contributing to the erosion rate and surface roughness of a titanium alloy prepared using a WJ was conducted. The general trends highlighted that:

- Supply pressure and traverse rate displayed the highest cumulative effect on the erosion rate and roughness parameters. From a process standpoint, in order to reduce exposure time, higher pressures must be considered.
- As the supply pressure increased, the degree of erosion (and roughness) increased.
- Standoff distances lower than 40 mm led to limited erosion at u ≥ 90 mm/s regardless of pressure.

- As the standoff distance increased from 40 mm to 100 mm, the erosion rates (and roughness parameters) increased in value. Further increases in standoff distance actually led to decreasing erosion.
- The regression analyses followed an exponential trend, due largely to the fact that threshold pressures were determined below which erosion was not initiated (for the given traverse rate ranges).
- The results of the water-air jet show that it may provide an effective means of controlling the jet structure – thus impacting the ability of the jet to remove material. Further classification of the water-air jet as a tool for surface texturing should be considered based on the preliminary results.

5. REFERENCES

[1] Hashish, M., Steele, D.E., and Bothell, D.H. "Machining with Super-Pressure (690 MPa) Waterjets." *International Journal of Machine Tools and Manufacturing*. Vol. 37, Issue 4, pp. 465 – 479, 1997.

[2] Hashish, M. "Cutting with Waterjets at 690 MPa." *ASME PVP: High Pressure Technology*. Volume 384, pp. 33-39, 1999.

[3] Hashish, M., et al, "Method and Apparatus for Fluidjet Formation, US patent number 6280302, August 2001.

[4] Kunaporn, S. and Ramulu, M. "Ultra High Pressure Waterjet Peening, Part I: Surface Texture." *Proceedings of the WJTA American Waterjet Conference: Volume 1*, 2001, pp. 90 – 95.

[5] Kunaporn, S., Chillman A., Ramulu, M., and Hashish, M. "Effect of waterjet formation on surface preparation and profiling of aluminum alloy." Wear. Vol. 265, pp. 176 – 185, 2008.

[6] Hashish, M. and Chillman, A. and Ramulu, M. "Waterjet Peening at 600 MPa: A First Investigation." *Proceedings of the IMECE: 2005 ASME Mechanical* Engineering Congress and Exposition. 2005.

[7] Chillman, A., Ramulu, M. and Hashish, M. "Waterjet Peening and Surface Preparation at 600 MPa: A Preliminary Experimental Study." ASME *Journal of Fluids Engineering*, Vol. 129, pp. 485 – 490, 2007.

[8] Momber, A.W. "Concrete failure due to air-water jet impingement." *Journal of Materials Science*, Vol. 35, pp. 2785 – 2789, 2000.

6. NOMENCLATURE

Air Flow Rate	q_a
Average Roughness	R_a
Coefficient of Discharge	C_D
Erosion Rate	E.R.
Orifice Diameter	d_n
Peak to Valley Roughness	R_y
Standoff Distance	h
Supply Pressure	P_S
Traverse Rate	u

7. EXPERIMENTAL TEST MATRICES

Table 2. Set #1 Experimental conditions.

Run	**Supply Pressure**	**Standoff**	**Traverse Rate**
(#)	*(MPa)*	*(mm)*	*(mm/s)*
1	275	25.4	30
2	275	25.4	90
3	275	25.4	150
4	275	38.1	30
5	275	38.1	90
6	275	38.1	150
7	275	50.8	30
8	275	50.8	90
9	275	50.8	150
10	414	25.4	30
11	414	25.4	90
12	414	25.4	150
13	414	38.1	30
14	414	38.1	90
15	414	38.1	150
16	414	50.8	30
17	414	50.8	90
18	414	50.8	150
19	600	25.4	30
20	600	25.4	90
21	600	25.4	150
22	600	38.1	30
23	600	38.1	90
24	600	38.1	150
25	600	50.8	30
26	600	50.8	90
27	600	50.8	150

Table 3. Set #2 Experimental conditions.

Run	**Supply Pressure**	**Standoff**	**Traverse Rate**
(#)	*(MPa)*	*(mm)*	*(mm/s)*
1	414	12.7	30
2	414	25.4	30
3	414	38.1	30
4	414	50.8	30
5	414	63.5	30
6	414	76.2	30
7	414	88.9	30
8	414	101.6	30
9	414	114.3	30
10	414	127	30
11	414	139.7	30
12	600	12.7	90
13	600	25.4	90
14	600	38.1	90
15	600	50.8	90
16	600	63.5	90
17	600	76.2	90
18	600	88.9	90
19	600	101.6	90
20	600	114.3	90
21	600	127	90
22	600	139.7	90

Table 4. Set #3 Experimental conditions.

Run	**Supply Pressure**	**Standoff**	**Traverse Rate**
(#)	(MPa)	(mm)	(mm/s)
1	414	12.7	90
2	414	38.1	90
3	414	63.5	90
4	414	88.9	90
5	414	114.3	90
6	414	139.7	90
7	600	12.7	30
8	600	38.1	30
9	600	63.5	30
10	600	88.9	30
11	600	114.3	30
12	600	139.7	30
13	600	12.7	150
14	600	38.1	150
15	600	63.5	150
16	600	88.9	150
17	600	114.3	150
18	600	139.7	150
19	275	50.8	30
20	275	101.6	30
21	275	101.6	90
22	275	101.6	150